JACS
JOURNAL OF THE AMERICAN CHEMICAL SOCIETY
pubs.acs.org/JACS
Communication

Metal Halide Perovskite Heterostructures: Blocking Anion Diffusion with Single-Layer Graphene

Matthew P. Hautzinger, Emily K. Raulerson, Steven P. Harvey, Tuo Liu, Daniel Duke, Xixi Qin, Rebecca A. Scheidt, Brian M. Wieliczka, Alan J. Phillips, Kenneth R. Graham, Volker Blum, Joseph M. Luther, Matthew C. Beard,* and Jeffrey L. Blackburn*

Cite This: J. Am. Chem. Soc. 2023, 145, 2052–2057

ABSTRACT: The development of metal halide perovskite/perovskite heterostructures is hindered by rapid interfacial halide diffusion leading to mixed alloys rather than sharp interfaces. To circumvent this outcome, we developed an ion-blocking layer consisting of single-layer graphene (SLG) deposited between the metal halide perovskite layers and demonstrated that it effectively blocks anion diffusion in a $CsPbBr_3$/SLG/$CsPbI_3$ heterostructure. Spatially resolved elemental analysis and spectroscopic measurements demonstrate the halides do not diffuse across the interface, whereas control samples without the SLG show rapid homogenization of the halides and loss of the sharp interface. Ultraviolet photoelectron spectroscopy, DFT calculations, and transient absorbance spectroscopy indicate the SLG has little electronic impact on the individual semiconductors. In the $CsPbBr_3$/SLG/$CsPbI_3$, we find a type I band alignment that supports transfer of photogenerated carriers across the heterointerface. Light-emitting diodes (LEDs) show electroluminescence from both the $CsPbBr_3$ and $CsPbI_3$ layers with no evidence of ion diffusion during operation. Our approach provides opportunities to design novel all-perovskite heterostructures to facilitate the control of charge and light in optoelectronic applications.

The ability to integrate semiconductors into heterostructure architectures is essential for enabling their use in a variety of optoelectronic applications. Advanced technologies typically integrate a variety of heterojunctions, homojunctions, etc., of conventional group IV and III–V semiconductors to enable a plethora of applications, such as photovoltaics, lasers, detectors, etc. In the case of metal halide perovskites (MHPs), heterostructures between various inorganic and organic semiconductors have enabled high-efficiency architectures, including photovoltaics,[1,2] LEDs,[3] and detectors/sensors.[4,5] However, expanding upon these heterostructures and interfacial chemistries to include all perovskite/perovskite heterostructures, thereby mimicking conventional semiconductor heterostructures, has proved to be challenging.[6−14]

Specifically, facile anion diffusion between MHPs prevents $APbX_3$/$APbX'_3$ heterostructure growth, where X and X′ are different halides. When two perovskites of different halide compositions are deposited sequentially and in direct contact, the halide ions rapidly diffuse to form alloys instead of sharp interfaces.[15−17] The resulting alloys lack the desirable properties of a sharp heterostructure interface, such as interfacial band alignment that facilitates control over carrier and energy transfer. This anion diffusion is so prominent that when a $MAPbI_3$ (MA = methylammonium) film is simply mechanically stacked onto a $MAPbBr_3$ film, the anions rapidly diffuse to form mixed compositions of $MAPb(Br_{3-x}I_x)$.[18] New approaches are needed to stabilize the composition of the heterostructures.

To solve the issue of halide mixing in MHPs, we looked to previous works on thin diffusion blocking materials. Previously, Bukola et al. showed single-layer graphene (SLG) acts as an ion diffusion blocking membrane in hydrogen pump cells, where protons pass through with high current densities; however, ions as small as potassium negligibly pass through the SLG.[19] This demonstration suggested that SLG could also be an effective barrier for blocking the large halide anions found in MHPs. In a few recent MHP studies, various forms of graphene have been incorporated as an additive into the electrodes[20−23] and transport layers[24−26] of MHP photovoltaics to enhance the overall stability characteristics. However, there has been little success integrating SLG within an all-perovskite/perovskite heterostructure[27] where the SLG serves as an ion diffusion blocking layer, and little is known regarding the degree to which such blocking layers impact optoelectronic properties and processes, such as charge/energy transfer. This is because most deposition conditions for graphene rely on polar solvents or require a high-temperature gas phase deposition, both of which degrade the MHP semiconductors.

To fabricate all-perovskite/perovskite heterostructures with SLG integrated as an ion diffusion blocking layer, we utilized a solvent-free transfer process of SLG to form stable $CsPbI_3$/SLG/$CsPbBr_3$ heterostructures.[19] SLG grown on copper foil

Received: November 22, 2022
Published: January 17, 2023

https://doi.org/10.1021/jacs.2c12441
J. Am. Chem. Soc. 2023, 145, 2052–2057

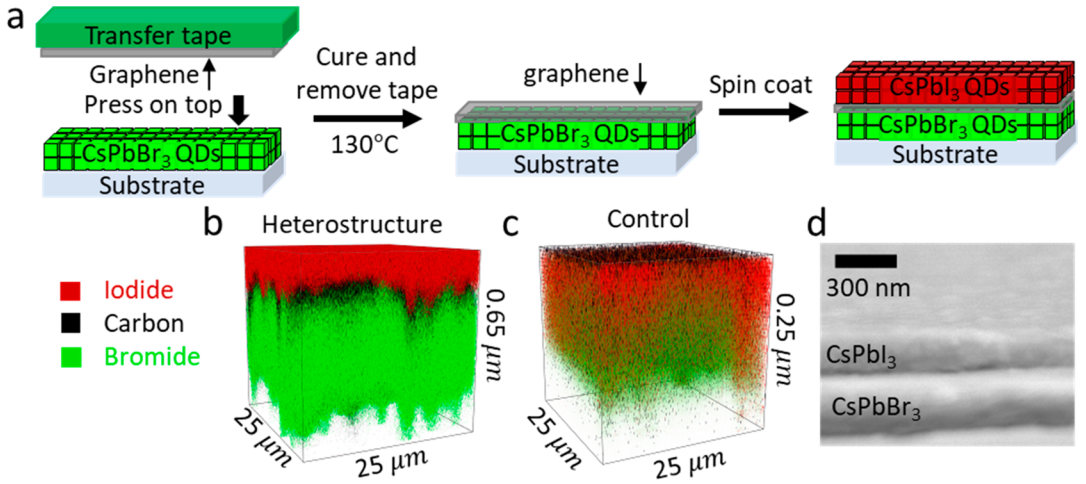

Figure 1. (a) Schematic of the single-layer graphene transfer process. TOF-SIMS 3D rendering (25 × 25 μm) of the (b) $CsPbBr_3$/SLG/$CsPbI_3$ heterostructure (depth, ~650 nm) and (c) control without the SLG, i.e., direct contact of the perovskite layers (depth, ~200 nm). (d) Cross section SEM image of the heterostructure.

was pressed onto a heat release transfer tape followed by removal of the Cu foil by etching in ammonium persulfate, which left behind a single layer of graphene. The SLG/heat transfer tape was then hot pressed at 130 °C onto a $CsPbBr_3$ nanocrystal (NC) film to cure the transfer tape and release the SLG from the tape and leave the SLG on top of the film (Figure 1a). Subsequently, a $CsPbI_3$ NC film was deposited by spin coating on top of the SLG to complete the $CsPbI_3$/SLG/$CsPbBr_3$ heterostructure.

Time of flight−secondary ion mass spectrometry (ToF-SIMS) measurements verify the retention of the separate halide ions across the perovskite layers in the SLG-incorporated heterostructure.[28] The $CsPbI_3$ layer remains isolated at the top of the film while the $CsPbBr_3$ layer remains at the bottom, with the SLG in between (compare red vs green shading in Figure 1b). In contrast, we find that the bromide and iodide anions rapidly mix throughout the film in the control sample of $CsPbBr_3$/$CsPbI_3$ deposited without the SLG (Figure 1c). Renderings of the individual ions and line profiles can be found in Figures S1 and S2. Cross-sectional SEM (Figure 1d) shows the heterostructure has a sharp interface between the perovskite films. Figure S3 shows the top view SEM images, Figure S4 shows AFM topography, and Figure S5 shows photographs of the heterostructure and control samples.

To further confirm that the SLG sufficiently blocks halide diffusion, we used UV−vis absorbance and photoluminescence (PL) spectroscopies. A film of only $CsPbBr_3$ NCs (Figure 2a, green traces) shows an absorption onset and PL emission at 520 nm, while a film of only $CsPbI_3$ NCs (Figure 2a, red traces) shows an absorption onset and PL emission at 680 nm. When the NCs are deposited without SLG as a control sample, the absorbance onset and PL emission rapidly merge and exhibit an absorption onset and PL at 630 nm (Figure 2a, yellow trace), as expected when the halides mix and form $CsPb(Br_{3-x}I_x)$.[17] The halide mixing across the heterointerface is fast and is completed in the time scales required to transfer the samples for measurement (<30 min).

In contrast, for the $CsPbBr_3$/SLG/$CsPbI_3$ heterostructure, discrete absorbance and PL features persist (Figure 2a, black trace) and match that of isolated samples (Figure 2a, red and green traces). This is strong evidence that the heterostructure does not undergo halide diffusion across the SLG.

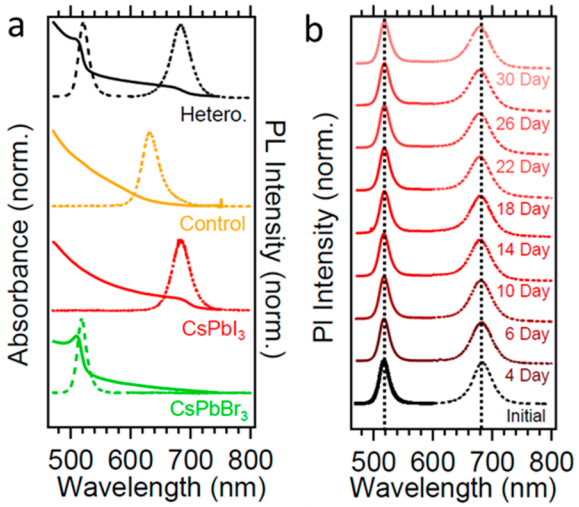

Figure 2. (a) Absorbance and PL spectra of control films of $CsPbBr_3$, $CsPbI_3$, and $CsPbBr_3$/$CsPbI_3$ deposited sequentially without the SLG (control), and of the heterostructure $CsPbBr_3$/SLG/$CsPbI_3$ (hetero.). (b) PL of the $CsPbBr_3$/SLG/$CsPbI_3$ heterostructure over the course of 30 days shows no evidence of halide intermixing, whereas the control sample is completely mixed almost instantaneously. Different dashed lines for spectra denote separate scans to probe the full wavelength range. Vertical dashed lines indicate initial positions of the two PL peaks.

Furthermore, we find that the PL peaks in a heterostructure sample stored at ambient conditions over 30 days show no clear evidence of shifting or change in the PL emission wavelengths (Figure 2b), thereby demonstrating that the SLG successfully blocks ion diffusion over long time scales.

The electronic properties of the $CsPbBr_3$/SLG/$CsPbI_3$ heterostructure were investigated with ultraviolet photoelectron spectroscopy (UPS). The alignment of the work functions of the MHP films with and without SLG (UPS spectra are shown in Figure S6) indicate that incorporating the SLG slightly raises the work functions of the NC films for both $CsPbI_3$ and $CsPbBr_3$ in a similar fashion, about 0.08−0.13 eV (compare right and left sides of Figure 3a). The measured work function of the SLG is slightly closer to vacuum than the VBs of both the $CsPbI_3$ and $CsPbBr_3$ (Figure 3a, left side).

https://doi.org/10.1021/jacs.2c12441
J. Am. Chem. Soc. 2023, 145, 2052−2057

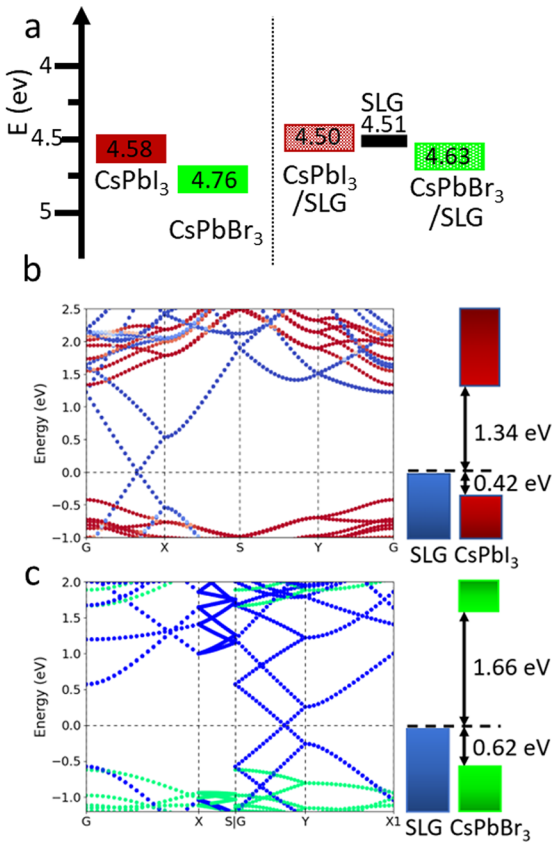

Figure 3. (a) Work functions versus vacuum (0 eV), as determined by UPS of the $CsPbI_3$ and $CsPbBr_3$ control samples and with the SLG showing the slight raising of the work function with SLG incorporation. The work function of the SLG is also shown. DFT band structure calculations of SLG incorporated with (b) $CsPbI_3$ and (c) $CsPbBr_3$. Schematics of the relaxed DFT structures are shown in Figure S6.

From previous reports, the $CsPbI_3/CsPbBr_3$ interface is expected to exhibit a type I band alignment.[9] Density functional theory (DFT) calculations corroborate this expectation. We used the FHI-aims code[29] to relax the (010)-oriented slab supercells of $CsPbI_3$ and $CsPbBr_3$ interfaced with SLG at the CsX-terminated surface[30] with the Perdew–Burke–Ernzerhof (PBE) semilocal density functional[31] and a version of the Tkatchenko–Scheffler (TS) dispersion correction[32] with a corrected van der Waals radius for Cs,[33] a $3 \times 1 \times 3$ *k*-point grid (SLG/$CsPbI_3$ slab), and a $1 \times 1 \times 1$ *k*-point grid (SLG/$CsPbBr_3$ slab). Then, the band structures were calculated with the hybrid HSE06 functional[34,35] with spin–orbit coupling[36] and with $4 \times 4 \times 4$ ($CsPbBr_3$) *k*-point grids. The perovskite lattices were matched to the PBE+TS optimized lattice parameter of SLG (2.46 Å) by straining the $CsPbI_3$ by 2.34% normal and 4.28% shear strain, and the $CsPbBr_3$ was strained by 0.70% normal and 3.35% shear strain (strain reported relative to the respective PBE+TS-optimized relaxed perovskite lattices). Calculations of two other supercells with different strain indicate that the impact of this strain on the predicted band gap is negligible (Figure S10).

The band structure calculations suggest a type I band alignment (Figure 3b,c) for the heterostructre. Furthermore, the Dirac point of the SLG falls inside the respective band gaps of the perovskites and close to the VB. Figures S7 and S8 show the DFT-relaxed models of the slab $CsPbX_3$/SLG structure, and Figure S9 shows the band structures of the bulk $CsPbX_3$ without SLG.

Transient absorbance spectroscopy (TAS) was used to probe the excited state dynamics of the heterostructure. Control experiments of individual $CsPbI_3$ (Figure 4a red open

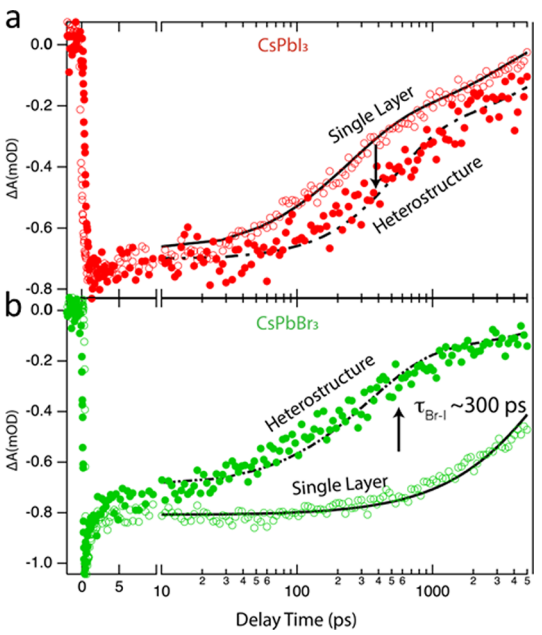

Figure 4. Transient absorbance spectroscopy of the $CsPbI_3$ (*a*) and $CsPbBr_3$ (b) control samples (with SLG integrated) in contrast to the $CsPbBr_3$/SLG/$CsPbI_3$ heterostructures. The black curve is the model for the single layer and heterostructure, where the $CsPbBr_3$ has shorter lifetimes, while the $CsPbI_3$ has longer lifetimes attributed to energy transfer.

circles) and $CsPbBr_3$ (Figure 4b, green open circles) NC films integrated with SLG characterize the decay of the excited state when carriers reside in $CsPbI_3$ or $CsPbBr_3$. When integrated into the $CsPbBr_3$/SLG/$CsPbI_3$ heterostructure, carriers within $CsPbBr_3$ decay faster relative to the control (compare green closed circles vs green open circles, Figure 4b). In contrast, carriers within $CsPbI_3$, when incorporated into the heterostructure, decay slower relative to the control $CsPbI_3$ (compare red closed circles to red open circles, Figure 3a).

The combination of the $CsPbBr_3$ exhibiting a faster decay of the ground state bleach while the $CsPbI_3$ decays slower suggests that photogenerated carriers can easily be transferred from the $CsPbBr_3$ to the $CsPbI_3$. We developed a simple transfer model to explain the data (black traces, Figure 3a,b). The decay rate within $CsPbBr_3$ and $CsPbI_3$ was characterized from the control experiments (solid black traces, Figure 4a,b). Then, the slower decay in the $CsPbI_3$ and faster decay in the $CsPbBr_3$ was simultaneously modeled by incorporating the transfer of carriers from the $CsPbBr_3$ to the $CsPbI_3$ (dashed black traces, Figure 4a,b). The transfer time was found via nonlinear least squares fitting to be ~300 ps.

Our data suggest that the SLG does not act as a significant source of carrier recombination because in our model of the TA experiment we account for all photogenerated charge carriers either recombining or transferring from the $CsPbBr_3$ to $CsPbI_3$, i.e., no other decay channel was needed to model our data. In addition, we can conclude that both carriers are able to transfer (i.e., equivalent to energy transfer) in agreement with a

https://doi.org/10.1021/jacs.2c12441
J. Am. Chem. Soc. 2023, 145, 2052–2057

type I band alignment because in the case of only charge transfer, we would expect the PL would quench in both films, which was not observed. Thus, the TAS results demonstrate the SLG does not hinder the electronic communication in between the perovskite layers.

To further probe the applicability of these heterostructures in a technologically relevant application, we fabricated LEDs with the $CsPbBr_3$/SLG/$CsPbI_3$ heterostructure. We observed stable electroluminescence from both $CsPbBr_3$ and $CsPbI_3$ (Figure S11). Because of processing conditions, the $CsPbI_3$ NC layer was kept thin and, thus, exhibited a weaker electroluminescence intensity relative to the $CsPbBr_3$. No mixing of the halides was observed, thereby confirming that the SLG enables optoelectronic-grade heterostructures.

We have developed a method to incorporate single-layer graphene at the interface between two MHP compositions and demonstrated that the SLG is an effective halide diffusion blocking layer; at the same time, the SLG does not degrade the optoelectronic properties of the perovskite semiconductors. The $CsPbBr_3$/SLG/$CsPbI_3$ heterostructures shown here show no signs of forming $CsPb(Br_{3-x}I_x)$ alloys, which form almost immediately without the SLG blocking layer. The solvent-free and mild SLG deposition conditions developed here should be versatile for fabricating various perovskite/perovskite architectures that are similar to more advanced conventional semiconductor architectures. Furthermore, our initial results from UPS, DFT, and TAS indicate that the SLG has little effect on the heterostructure's electronic behavior, which exhibits a type I band alignment that promotes energy transfer between the layers, thereby indicating electronic communication between the heterostructure components. This provides opportunities to integrate MHP semiconductors into targeted applications.

■ ASSOCIATED CONTENT

Supporting Information

The Supporting Information is available free of charge at https://pubs.acs.org/doi/10.1021/jacs.2c12441.

Experimental details, ToF-SIMS data, SEM images, photographs, UPS spectra, electroluminescence data, and DFT details (PDF)

■ AUTHOR INFORMATION

Corresponding Authors

Matthew C. Beard − *National Renewable Energy Laboratory, Golden, Colorado 80401, United States;* orcid.org/0000-0002-2711-1355; Email: Matt.beard@nrel.gov

Jeffrey L. Blackburn − *National Renewable Energy Laboratory, Golden, Colorado 80401, United States;* orcid.org/0000-0002-9237-5891; Email: jeffrey.blackburn@nrel.gov

Authors

Matthew P. Hautzinger − *National Renewable Energy Laboratory, Golden, Colorado 80401, United States;* orcid.org/0000-0002-4764-3076

Emily K. Raulerson − *National Renewable Energy Laboratory, Golden, Colorado 80401, United States*

Steven P. Harvey − *National Renewable Energy Laboratory, Golden, Colorado 80401, United States;* orcid.org/0000-0001-6120-7062

Tuo Liu − *Department of Chemistry, University of Kentucky, Lexington, Kentucky 40506, United States*

Daniel Duke − *Thomas Lord Department of Mechanical Engineering and Material Science, Duke University, Durham, North Carolina 27708, United States*

Xixi Qin − *Thomas Lord Department of Mechanical Engineering and Material Science, Duke University, Durham, North Carolina 27708, United States*

Rebecca A. Scheidt − *National Renewable Energy Laboratory, Golden, Colorado 80401, United States*

Brian M. Wieliczka − *National Renewable Energy Laboratory, Golden, Colorado 80401, United States*

Alan J. Phillips − *National Renewable Energy Laboratory, Golden, Colorado 80401, United States;* orcid.org/0000-0002-7529-4379

Kenneth R. Graham − *Department of Chemistry, University of Kentucky, Lexington, Kentucky 40506, United States;* orcid.org/0000-0002-6387-3998

Volker Blum − *Thomas Lord Department of Mechanical Engineering and Material Science, Duke University, Durham, North Carolina 27708, United States;* orcid.org/0000-0001-8660-7230

Joseph M. Luther − *National Renewable Energy Laboratory, Golden, Colorado 80401, United States;* orcid.org/0000-0002-4054-8244

Complete contact information is available at: https://pubs.acs.org/10.1021/jacs.2c12441

Notes

The authors declare no competing financial interest.

■ ACKNOWLEDGMENTS

This work was supported by the Center for Hybrid Organic Inorganic Semiconductors for Energy (CHOISE), an Energy Frontier Research Center funded by the Office of Basic Energy Sciences, Office of Science within the U.S. Department of Energy through contract number DE-AC36-08G028308. The views expressed in the article do not necessarily represent the views of the DOE or the U.S. Government. T.L. and K.R.G. ackknowledge support from the National Science Foundation (award number OIA-1929131) for ultraviolet phoelectron spectroscopy measurements. D.D. carried out DFT simulations as part of a Research Experience for Undergraduate students program supported by the National Science Foundation (award numbers 2050900, 2050841, and 2050764 and ECCS-2025064). Any opinions, findings, and conclusions or recommendations expressed in this material do not necessarily reflect the views of the National Science Foundation. This research used resources of the National Energy Research Scientific Computing Center (NERSC), a U.S. Department of Energy (DOE) Office of Science User Facility operated under Contract no. DEAC02-05CH11231.

■ REFERENCES

(1) Kojima, A.; Teshima, K.; Shirai, Y.; Miyasaka, T. Organometal Halide Perovskites as Visible-Light Sensitizers for Photovoltaic Cells. *J. Am. Chem. Soc.* **2009**, *131* (17), 6050−6051.

(2) Lee, M. M.; Teuscher, J.; Miyasaka, T.; Murakami, T. N.; Snaith, H. J. Efficient Hybrid Solar Cells Based on Meso-Superstructured Organometal Halide Perovskites. *Science* **2012**, *338* (6107), 643−647.

(3) Schulz, P.; Cahen, D.; Kahn, A. Halide Perovskites: Is It All about the Interfaces? *Chem. Rev.* **2019**, *119* (5), 3349−3417.

(4) Hao, J.; Lu, H.; Mao, L.; Chen, X.; Beard, M. C.; Blackburn, J. L. Direct Detection of Circularly Polarized Light Using Chiral Copper Chloride−Carbon Nanotube Heterostructures. *ACS Nano* **2021**, *15* (4), 7608−7617.
(5) Hao, J.; Kim, Y.-H.; Habisreutinger, S. N.; Harvey, S. P.; Miller, E. M.; Foradori, S. M.; Arnold, M. S.; Song, Z.; Yan, Y.; Luther, J. M.; Blackburn, J. L. Low-Energy Room-Temperature Optical Switching in Mixed-Dimensionality Nanoscale Perovskite Heterojunctions. *Science Advances* **2021**, *7* (18), eabf1959.
(6) Ortiz-Cervantes, C.; Carmona-Monroy, P.; Solis-Ibarra, D. Two-Dimensional Halide Perovskites in Solar Cells: 2D or Not 2D? *ChemSusChem* **2019**, *12* (8), 1560−1575.
(7) Kennard, R. M.; Dahlman, C. J.; Nakayama, H.; DeCrescent, R. A.; Schuller, J. A.; Seshadri, R.; Mukherjee, K.; Chabinyc, M. L. Phase Stability and Diffusion in Lateral Heterostructures of Methyl Ammonium Lead Halide Perovskites. *ACS Appl. Mater. Interfaces* **2019**, *11* (28), 25313−25321.
(8) Roy, C. R.; Pan, D.; Wang, Y.; Hautzinger, M. P.; Zhao, Y.; Wright, J. C.; Zhu, Z.; Jin, S. Anion Exchange of Ruddlesden−Popper Lead Halide Perovskites Produces Stable Lateral Heterostructures. *J. Am. Chem. Soc.* **2021**, *143* (13), 5212−5221.
(9) Liu, C.; Hu, M.; Zhou, X.; Wu, J.; Zhang, L.; Kong, W.; Li, X.; Zhao, X.; Dai, S.; Xu, B.; Cheng, C. Efficiency and Stability Enhancement of Perovskite Solar Cells by Introducing CsPbI3 Quantum Dots as an Interface Engineering Layer. *NPG Asia Materials* **2018**, *10* (6), 552−561.
(10) Pan, D.; Fu, Y.; Spitha, N.; Zhao, Y.; Roy, C. R.; Morrow, D. J.; Kohler, D. D.; Wright, J. C.; Jin, S. Deterministic Fabrication of Arbitrary Vertical Heterostructures of Two-Dimensional Ruddlesden−Popper Halide Perovskites. *Nat. Nanotechnol.* **2021**, *16* (2), 159−165.
(11) Akriti; Shi, E.; Shiring, S. B.; Yang, J.; Atencio-Martinez, C. L.; Yuan, B.; Hu, X.; Gao, Y.; Finkenauer, B. P.; Pistone, A. J.; Yu, Y.; Liao, P.; Savoie, B. M.; Dou, L. Layer-by-Layer Anionic Diffusion in Two-Dimensional Halide Perovskite Vertical Heterostructures. *Nat. Nanotechnol.* **2021**, *16* (5), 584−591.
(12) Akriti; Zhang, S.; Lin, Z.-Y.; Shi, E.; Finkenauer, B. P.; Gao, Y.; Pistone, A. J.; Ma, K.; Savoie, B. M.; Dou, L. Quantifying Anionic Diffusion in 2D Halide Perovskite Lateral Heterostructures. *Adv. Mater.* **2021**, *33* (51), 2105183.
(13) Dou, L.; Lai, M.; Kley, C. S.; Yang, Y.; Bischak, C. G.; Zhang, D.; Eaton, S. W.; Ginsberg, N. S.; Yang, P. Spatially Resolved Multicolor CsPbX3 Nanowire Heterojunctions via Anion Exchange. *Proc. Natl. Acad. Sci. U. S. A.* **2017**, *114* (28), 7216−7221.
(14) Shi, E.; Yuan, B.; Shiring, S. B.; Gao, Y.; Akriti; Guo, Y.; Su, C.; Lai, M.; Yang, P.; Kong, J.; Savoie, B. M.; Yu, Y.; Dou, L. Two-Dimensional Halide Perovskite Lateral Epitaxial Heterostructures. *Nature* **2020**, *580* (7805), 614−620.
(15) Hoke, E. T.; Slotcavage, D. J.; Dohner, E. R.; Bowring, A. R.; Karunadasa, H. I.; McGehee, M. D. Reversible Photo-Induced Trap Formation in Mixed-Halide Hybrid Perovskites for Photovoltaics. *Chem. Sci.* **2015**, *6* (1), 613−617.
(16) Pan, D.; Fu, Y.; Chen, J.; Czech, K. J.; Wright, J. C.; Jin, S. Visualization and Studies of Ion-Diffusion Kinetics in Cesium Lead Bromide Perovskite Nanowires. *Nano Lett.* **2018**, *18* (3), 1807−1813.
(17) Akkerman, Q. A.; D'Innocenzo, V.; Accornero, S.; Scarpellini, A.; Petrozza, A.; Prato, M.; Manna, L. Tuning the Optical Properties of Cesium Lead Halide Perovskite Nanocrystals by Anion Exchange Reactions. *J. Am. Chem. Soc.* **2015**, *137* (32), 10276−10281.
(18) Elmelund, T.; Scheidt, R. A.; Seger, B.; Kamat, P. V. Bidirectional Halide Ion Exchange in Paired Lead Halide Perovskite Films with Thermal Activation. *ACS Energy Lett.* **2019**, *4* (8), 1961−1969.
(19) Bukola, S.; Liang, Y.; Korzeniewski, C.; Harris, J.; Creager, S. Selective Proton/Deuteron Transport through Nafion|Graphene|Nafion Sandwich Structures at High Current Density. *J. Am. Chem. Soc.* **2018**, *140* (5), 1743−1752.
(20) You, P.; Liu, Z.; Tai, Q.; Liu, S.; Yan, F. Efficient Semitransparent Perovskite Solar Cells with Graphene Electrodes. *Adv. Mater.* **2015**, *27* (24), 3632−3638.
(21) Lin, X.; Su, H.; He, S.; Song, Y.; Wang, Y.; Qin, Z.; Wu, Y.; Yang, X.; Han, Q.; Fang, J.; Zhang, Y.; Segawa, H.; Grätzel, M.; Han, L. In Situ Growth of Graphene on Both Sides of a Cu−Ni Alloy Electrode for Perovskite Solar Cells with Improved Stability. *Nature Energy* **2022**, *7*, 520.
(22) Lang, F.; Gluba, M. A.; Albrecht, S.; Rappich, J.; Korte, L.; Rech, B.; Nickel, N. H. Perovskite Solar Cells with Large-Area CVD-Graphene for Tandem Solar Cells. *J. Phys. Chem. Lett.* **2015**, *6* (14), 2745−2750.
(23) Yoon, J.; Sung, H.; Lee, G.; Cho, W.; Ahn, N.; Jung, H. S.; Choi, M. Superflexible, High-Efficiency Perovskite Solar Cells Utilizing Graphene Electrodes: Towards Future Foldable Power Sources. *Energy Environ. Sci.* **2017**, *10* (1), 337−345.
(24) O'Keeffe, P.; Catone, D.; Paladini, A.; Toschi, F.; Turchini, S.; Avaldi, L.; Martelli, F.; Agresti, A.; Pescetelli, S.; Del Rio Castillo, A. E.; Bonaccorso, F.; Di Carlo, A. Graphene-Induced Improvements of Perovskite Solar Cell Stability: Effects on Hot-Carriers. *Nano Lett.* **2019**, *19* (2), 684−691.
(25) Koo, D.; Kim, U.; Cho, Y.; Lee, J.; Seo, J.; Choi, Y.; Choi, K. J.; Baik, J. M.; Yang, C.; Park, H. Graphene-Assisted Zwitterionic Conjugated Polycyclic Molecular Interfacial Layer Enables Highly Efficient and Stable Inverted Perovskite Solar Cells. *Chem. Mater.* **2021**, *33* (14), 5563−5571.
(26) Biccari, F.; Gabelloni, F.; Burzi, E.; Gurioli, M.; Pescetelli, S.; Agresti, A.; Del Rio Castillo, A. E.; Ansaldo, A.; Kymakis, E.; Bonaccorso, F.; Di Carlo, A.; Vinattieri, A. Graphene-Based Electron Transport Layers in Perovskite Solar Cells: A Step-Up for an Efficient Carrier Collection. *Adv. Energy Mater.* **2017**, *7* (22), 1701349.
(27) Gong, K.; Hu, J.; Cui, N.; Xue, Y.; Li, L.; Long, G.; Lin, S. The Roles of Graphene and Its Derivatives in Perovskite Solar Cells: A Review. *Materials & Design* **2021**, *211*, 110170.
(28) Harvey, S. P.; Messinger, J.; Zhu, K.; Luther, J. M.; Berry, J. J. Investigating the Effects of Chemical Gradients on Performance and Reliability within Perovskite Solar Cells with TOF-SIMS. *Adv. Energy Mater.* **2020**, *10* (26), 1903674.
(29) Blum, V.; Gehrke, R.; Hanke, F.; Havu, P.; Havu, V.; Ren, X.; Reuter, K.; Scheffler, M. Ab Initio Molecular Simulations with Numeric Atom-Centered Orbitals. *Comput. Phys. Commun.* **2009**, *180* (11), 2175−2196.
(30) Chen, Y.; Smock, S. R.; Flintgruber, A. H.; Perras, F. A.; Brutchey, R. L.; Rossini, A. J. Surface Termination of CsPbBr3 Perovskite Quantum Dots Determined by Solid-State NMR Spectroscopy. *J. Am. Chem. Soc.* **2020**, *142* (13), 6117−6127.
(31) Perdew, J. P.; Burke, K.; Ernzerhof, M. Generalized Gradient Approximation Made Simple. *Phys. Rev. Lett.* **1996**, *77* (18), 3865−3868.
(32) Tkatchenko, A.; Scheffler, M. Accurate Molecular Van Der Waals Interactions from Ground-State Electron Density and Free-Atom Reference Data. *Phys. Rev. Lett.* **2009**, *102* (7), 073005.
(33) Kim, Y.-H.; Song, R.; Hao, J.; Zhai, Y.; Yan, L.; Moot, T.; Palmstrom, A. F.; Brunecky, R.; You, W.; Berry, J. J.; et al. The Structural Origin of Chiroptical Properties in Perovskite Nanocrystals with Chiral Organic Ligands. *Advanced Functional Materials* **2022**, *32* (25), 2200454.
(34) Heyd, J.; Scuseria, G. E.; Ernzerhof, M. Hybrid Functionals Based on a Screened Coulomb Potential. *J. Chem. Phys.* **2003**, *118* (18), 8207−8215.
(35) Heyd, J.; Scuseria, G. E.; Ernzerhof, M. Erratum: "Hybrid Functionals Based on a Screened Coulomb Potential" [J. Chem. Phys. 118, 8207 (2003)]. *J. Chem. Phys.* **2006**, *124* (21), 219906.
(36) Huhn, W. P.; Blum, V. One-Hundred-Three Compound Band-Structure Benchmark of Post-Self-Consistent Spin-Orbit Coupling Treatments in Density Functional Theory. *Phys. Rev. Materials* **2017**, *1* (3), 033803.

https://doi.org/10.1021/jacs.2c12441
J. Am. Chem. Soc. 2023, 145, 2052−2057

NOTE ADDED AFTER ASAP PUBLICATION

This paper was published January 17, 2023, with the incorrect Figure 4. The corrected version was reposted on January 18, 2023.

https://doi.org/10.1021/jacs.2c12441
J. Am. Chem. Soc. 2023, 145, 2052−2057